Robustly Adjusting Indoor Drip Irrigation Emitters with the Toyota HSR Robot

Ron Berenstein[1], Roy Fox[2], Stephen McKinley[3], Stefano Carpin[4], and Ken Goldberg[1,2,5]

***Abstract*— Indoor plants in homes and commercial buildings such as malls, offices, airports, and hotels, can benefit from precision irrigation to maintain healthy growth and reduce water consumption. As active valves are too costly, and ongoing precise manual adjustment of drip emitters is impractical, we explore how the Toyota HSR mobile manipulator robot can autonomously adjust low-cost passive emitters. To provide sufficient accuracy for gripper alignment, we designed a lightweight, modular Emitter Localization Device (ELD) with cameras and LEDs that can be non-invasively mounted on the arm. This paper presents details of the design, algorithms, and experiments with adjusting emitters using a two-phase procedure: 1) aligning the robot base using the build-in hand camera, and 2) aligning the gripper axis with the emitter axis using the ELD. We report success rates and sensitivity analysis to tune computer vision parameters and joint motor gains. Experiments suggest that emitters can be adjusted with 95% success rate in approximately 20 seconds.**

I. Introduction

Drip irrigation is the most widespread and well-known irrigation method in agriculture, whereby water is delivered to the plants via a network of perforated tubes [1]. The amount of water delivered to each plant is regulated by setting the irrigation timing — frequency and duration — and by choosing the flow-rate of the drip irrigation emitter. *Precision irrigation* is the selective control of individual plants' irrigation levels based on its needs.

The challenge of indoor precision irrigation is that physical conditions can be highly variable between plants, often even in the same proximity [2]. Plants irrigated by the same tube may have different morphology, lighting, air flow, or drainage, and therefore have different water-stress levels under the same irrigation schedule. Near-infrared and thermal sensing technologies can measure water-stress levels, indicating the amount of water the plant needs [3]. Precision irrigation then has the potential to close the sensing–actuation loop, and optimize and equalize water-stress levels across plants at the single-plant resolution. This would prevent over-watering, reduce fresh water usage, and increase plant vitality.

To adjust the irrigation level per plant we propose using adjustable passive flow-rate drip irrigation emitters (Figure 1b, 2b) which cost under $0.30. The flow-rate can be changed by rotating the emitter cap. This is much more cost effective than active irrigation valves at about $30 per unit.

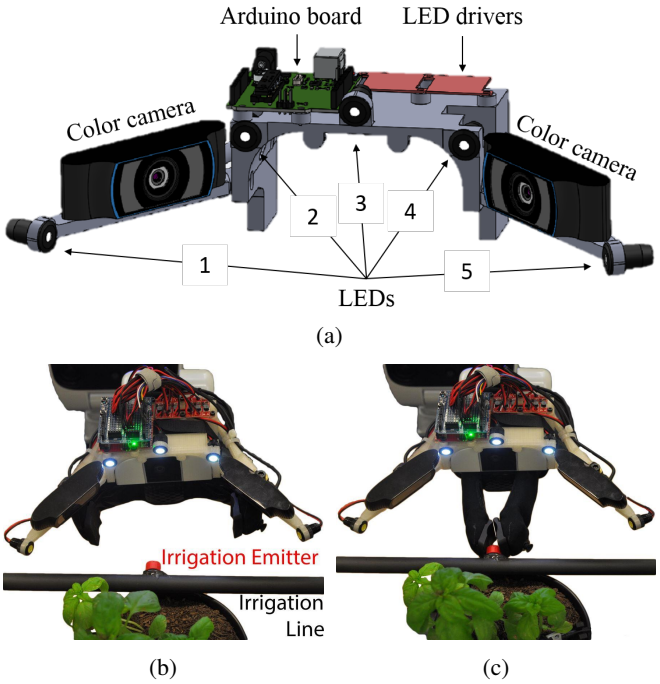

Fig. 1: Emitter Localization Device (ELD). (a) Front view of the CAD model of the ELD. Mounted on the ELD body are two color cameras facing inwards, five LEDs, an Arduino board, and LED drivers. (b) ELD mounted on a Toyota Human Support Robot (HSR) gripper using a Velcro strap. (c) The HSR grasping the red cap of a drip irrigation emitter.

In this paper we present a novel approach to adjusting emitters using an autonomous mobile robotic manipulator. We propose a procedure where the robot positions its base in front of an emitter, then reaches the emitter, grasps it, and rotates the emitter cap to the desired angle.

We present the Emitter Localization Device (ELD), a custom sensing and lighting system that is mountable on a manipulator having a parallel jaw gripper. We also propose vision and control algorithms for autonomously reaching and grasping emitters. We implemented this approach on a Toyota Human Support Robot (HSR[1]), and used it to tune parameters and evaluate the system in experiments reported in this paper.

This paper makes three contributions:

1) **Emitter Localization Device (ELD)**. We present a

The AUTOLAB at UC Berkeley; autolab.berkeley.edu
[1]CITRIS, [2]EECS, [3]ME, [5]IEOR, UC Berkeley, CA, USA
[4]School of Engineering, UC Merced, CA, USA
{ron.berenstein, royf, mckinley, goldberg}@berkeley.edu
scarpin@ucmerced.edu

[1]http://www.toyota-global.com/innovation/partner_robot/family_2.html

detachable stereo camera device designed to facilitate the detection of adjustable drip irrigation emitters in indoor environments, with two color cameras and five controllable light sources (Figure 1).

2) **Vision algorithm for localizing irrigation emitters**. We propose a machine-vision algorithm for detecting the position and orientation of emitters in lateral images from the two ELD cameras. We test different light intensities and configurations.
3) **Robot positioning, reaching, and grasping algorithm**. We propose an algorithm for controlling a mobile robotic manipulator to approach and grasp drip emitters based on visual feedback from the ELD cameras.

The paper is organized as follows: Section II discusses related work and the current state of the art. Section III defines the problem, assumptions, and limitations. Section IV presents the methods we propose, including the developed device and the vision and control algorithms. Section V overviews the autonomous system for adjusting emitters. Section VI describes the experiments conducted to evaluate the approach.

II. Related Work

To the best of our knowledge there are currently no robotic systems that directly address precision irrigation in indoor settings.

A. Adjusting indoor plant irrigation levels

Indoor growing operations exist in scales ranging from in-home gardens, to distributed urban farms [4], to vast indoor warehouses [5].

Unmanned Ground Vehicles (UGVs) and robotic arms have been used in a variety of automated growing systems. A UGV with an in-hand camera and vision for indoor tomato growing was demonstrated by Correll et al. [6] and Nagaraja et al. [7], with irrigation dispensed from an on-board water container. The iPlant robot [8] is an indoor UGV with several different tools and attachments for plant manipulation along greenhouse rows. Autonomous vision-based indoor harvesting of tomatoes was demonstrated by Taqi et al. [9]. An industrial Kuka robot arm with in-hand cameras and lighting was used for indoor irrigation by Scharr et al. [10].

Gealy et al. [11] developed the DATE (Device for Automated Tuning of Emitters), a hand-held device that can systematically adjust emitters. The device was designed for a human worker to attach it to an emitter to adjust the emitter's flow-rate, based on location-specific information provided by a cloud-based control algorithm that determines desired irrigation levels based on UAV-collected data. The DATE addresses the problem of accurately adjusting the emitter cap, however a human operator needs to reach each emitter, which is highly time-consuming when hundreds of emitters are to be adjusted.

B. Object detection in plant-growing environments

A key challenge in precision irrigation is active exploration, which involves positioning the robot's sensors to obtain measurements that reduce uncertainty in the state of the robot and the environment [12], [13], [14].

Lottes et al. [15] used feature extraction and near-infrared (NIR) imaging to separate plant leaves from a soil background. An industrial-scale farm robot was recently developed by Bawden et al. [16] which used a combination of RGB and NIR cameras to separate weeds from crops. Botterill et al. [17] addressed the lighting and perception problem by constructing a mobile 3.5m$\times$2m$\times$2.5m 'room' containing lights and a robotic arm that moves along the length of a vineyard row to harvest grapes.

Recently, Bargoti et al. [18] successfully used a multi-layer perceptron for fruit detection and localization in orchards with a single RGB camera, a task reminiscent of emitter detection. However, it remains unclear whether this approach can yield sufficient positional accuracy for object interaction in real settings.

C. Robotic manipulation in outdoor environments

Silwal et al. [19] recently developed an apple-picking robotic platform consisting of a custom arm and hand mounted on an all-terrain vehicle. A similar custom apparatus for indoor growing applications was created by Bac et al. [20], that consisted of a rail-mounted system that moves between rows of bell peppers in a greenhouse. Both of these approaches are potentially limited by custom single-purpose hardware if the problem includes plants in an unstructured environment.

A UGV with a robotic arm such as the Toyota HSR can be used for a multitude of tasks [21]. Small UGVs with simple manipulators have been deployed for weed retrieval [22], weed detection [23], and precision herbicide deployment [24], [25].

Large-scale UGVs operating in distributed systems have been used for outdoor agricultural settings [26] and implemented as autonomous tractors for outdoor harvesting [27], [28]. With inexpensive computer vision sensors, global positioning systems, LIDAR, and Inertial Measurement Units (IMUs), robotics research over the past two decades have led to many examples of autonomous robotic vehicles in agriculture [29].

III. Problem Statement

A. Definition and Notation

We study the problem of adjusting drip irrigation emitters in an indoor environment using a mobile robotic manipulator. The objective is to maximize success rate and speed. Success is defined as reaching a specified emitter, grasping it approximately in line with its rotation axis, and rotating it a specified angle.

A further requirement is the modularity of the hardware modification of the robotic manipulator. In particular, it should be easy to redesign the device to fit other robotic

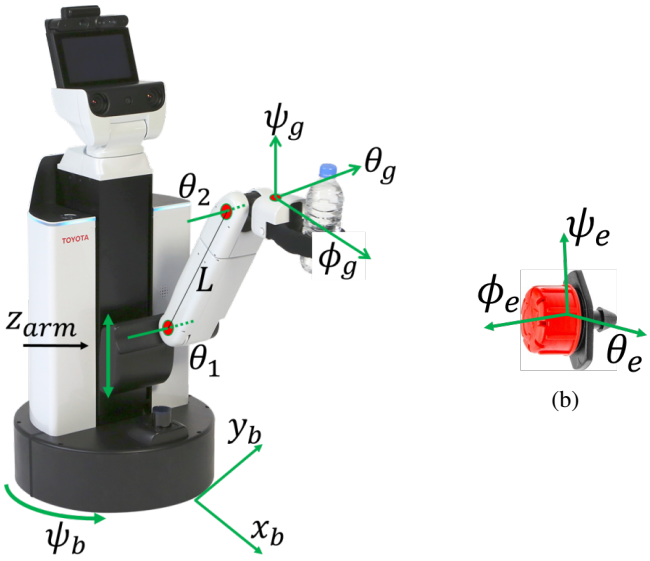

(a) (b)

Fig. 2: Notation of rotation and translation axes for (a) the HSR base, arm, and gripper; and (b) the adjustable emitter.

manipulators; mounting the device should be easy and removable without impacting the main hardware; the design should reduce imprecision in mounting and the algorithms should tolerate the remaining imprecision; the device should be lightweight; and communication and power should be supplied separately from the main hardware.

The mobile robotic manipulator we use, a Toyota Human Support Robot (HSR), consists of an omnidirectional moving base with a laser scanner, and an arm with a wide-angle in-hand camera and a parallel jaw gripper (see Figure 2). With respect to a fixed coordinate frame $(\vec{x}, \vec{y}, \vec{z})$, we denote the absolute base position and horizontal orientation (yaw) by (x_b, y_b, ψ_b), and the gripper position and vertical orientation (pitch) by $(x_g, y_g, z_g, \theta_g)$. The arm of the Toyota HSR cannot rotate horizontally independently of the base, and only ψ_b controls the gripper's yaw $\psi_g = \psi_b$. The gripper's roll ϕ_g is only used to adjust the emitter.

The database of emitter cap locations and rotations (rolls) is denoted by $\{(x_e^i, y_e^i, z_e^i, \phi_e^i) : \ 1 \leq i \leq n\}$, where n is the number of emitters. Each emitter has an unknown pitch θ_e^i. The robot is issued a sequence of adjustment commands of the form $(x_e^i, y_e^i, z_e^i, \Delta\phi)$, directing it to rotate emitter i by an angle $\Delta\phi$. While handling emitter i, we simplify the notation by defining the positive x axis to be directed towards the emitter, i.e., the emitter's yaw is always $\psi_e^i = 180°$.

B. Assumptions

We assume each plant is irrigated by a single adjustable drip emitter with a red cap that is attached to a black irrigation tube. We also assume that the plant are green without red hue flowers. We assume that each emitter is clearly visible to the robot's in-hand camera at distances below its initial distance of roughly 43cm, under existing light conditions. We also assume that no other red objects

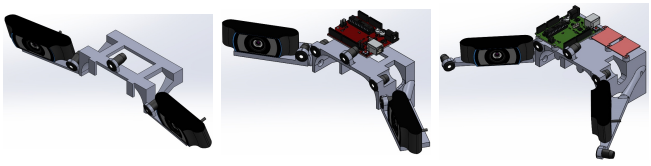

(a) (b) (c)

Fig. 3: ELD prototypes. (a) Prototype A: wide camera angles (˜90° from the ELD's symmetry plane) with three LEDs pointing forward. (b) Prototype B: camera angles of 25° with five LEDs. (c) Prototype C: this model was used in the experiments; camera angles of 45° and five LEDs. Three LEDs are pointing forward and two sideways. LEDs are positioned on either side of each camera to allow experiments with different light configurations.

are visible to the robot during the task. We assume that the emitter locations in the database are accurate to within 10cm, which is less than half the distance between emitters, allowing the robot to uniquely identify each specified emitter by cropping input image to include exactly one emitter.

The plants, irrigation tube, and emitters, are set on a rack of known width, that is assumed to have a base surface detectable by the robot's laser scanner. Since we define the positive x axis to be directed towards the emitters and plant rack, the base surface of the rack is in the yz plane. When the robot faces perpendicular to the rack, i.e., $\psi_b \simeq 0$, it can successfully rotate an emitter if the emitter's and gripper's rotation axes ϕ are approximately in line, i.e., their pitches θ_e and θ_g differ by $180° \pm 3°$. We assume that the gripper's range allows it to reach these pitch values for all emitters, which are between $-20°$ and $+20°$.

IV. Methods

We use the Toyota Human Support Robot (HSR) (Figure 2, 6b), which consists of an omnidirectional mobile platform with a maximum speed of 0.22 m/s, a 5-DoF robotic arm that can reach 450mm in depth and 0–1350mm in height with payload of 1.2kg, and a parallel jaw gripper (Figure 1). The sensors of the HSR include stereo vision, an RGB-D camera, two wide-angle cameras (in head and in hand), a laser scanner, and more. In this work we only use the wide-angle in-hand camera and the laser scanner.

A. Emitter Localization Device

We designed an Emitter Localization Device (ELD) to facilitate the detection and localization of adjustable emitters. The body of the ELD is designed as a mount for cameras and lighting equipment on the robot's hand. Since the robotic platform being used in this work is the Toyota HSR, the ELD body was design specifically to fit the HSR hand (Figure 1). The ELD is attached securely to the top part of the HSR hand using a Velcro strap. This design makes attaching and detaching the ELD easy, fast, and reversible without impacting the main HSR hardware.

The ELD body is assembled from two parts: the main body used for mounting on the HSR hand and for carrying the

electronics and lights, and wings used to carry the cameras and lights (Figure 3). Two principles guided the design of the ELD. On the one hand, we prefer for the cameras to point sideways to the emitter for enhanced identifiability of the emitter pitch θ_e: when a cylinder is viewed from the side, the resulting image is a rectangle whose upper and lower sides are slanted in parallel to the cylinder's rotation axis (Figure 4). On the other hand, we prefer to locate the cameras as posterior as possible on the device to avoid collisions with obstacles while approaching the emitter, and to allow free rotation of the emitter while grasping (Figure 1c). The evolution of the ELD included the design, manufacturing, and evaluation of three prototypes that differently trade off these two principles (Figure 3). The main variability between these prototypes is in the horizontal angle of the cameras and the number of light sources and their positions.

For the experiments presented in Section VI we choose Prototype C (Figure 3c) since this model allows safe rotation of the emitter cap, while the camera angles facilitate reliable detection of the emitter's pitch θ_e. Light sources on either side of each camera allowed us to experiment with different light configurations, as detailed in Section IV-B.

The body of the ELD is 3D-printed using PLA material. The printing volume is 137.2cm^3 and the printed weight is 166g and the total weight is 280g. Two color cameras (Logitech c920, resolution 480×640) are positioned inward to view the adjustable emitter from two sides, which enables detection of the emitter's edges to determine its pitch θ_e. Five spot LEDs (12v, 0.5W) are mounted to provide consistent lighting around the gripper. A single LED lights the front of the detected object (Figure 1a, LED 3), while one more LED on either side of each camera add to the light coverage of the object from each camera's point of view (Figure 1a, LEDs 1–2, 4–5). The light intensity of each LED is set by a microcontroller board (Arduino Uno) and LED drivers (PicoBuck) (Figures 1a). The device can be adapted to fit other robotic arms and end effectors by redesigning the body of the ELD and re-positioning the cameras and the light sources.

B. Emitter detection algorithm

We use color thresholding, edge detection, and the Hough transform to localize emitters. The vision algorithm is applied to the RGB images captured from each inward ELD camera (Figure 4 lower-left inset), and its output is the detected emitter's center of mass and orientation in pixel space (x_p, y_p, α_p). These correspond, through calibration (Section V-A), to the relative translation and pitch rotation between the gripper and the emitter, $(x_e - x_g)$, $(z_e - z_g)$, and $(\theta_e - \theta_g)$, and are later used to plan the motion of the robot gripper (Section V-B).

The algorithm operates in two steps: the first detects the silhouette of the emitter in the image, and the second determines its position and orientation. The detection step is based on identifying all large red regions of the image, and choosing the one with the highest red hue value. Detection operates as follows:

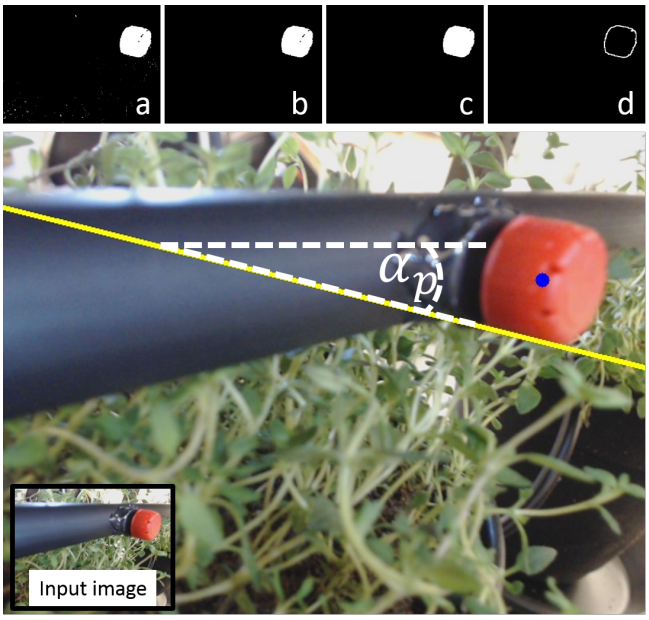

Fig. 4: Emitter detection algorithm. Lower-left inset: input image. (a) Extract red regions. (b) Remove small objects as noise. (c) Extract the object with the highest red hue value and its center of mass. (d) Apply the Canny edge detector and the Hough transform to find straight lines. Center: algorithm's output, emitter center of mass (x_p, y_p) depicted by the blue dot, and orientation α_p depicted by the slope of the yellow line.

1) Extract red regions in the image by creating two channel-ratio masks, red–green and red–blue, and filter by a threshold c on their sum, i.e., $({}^{red}/_{green} + {}^{red}/_{blue}) > c$ (Figure 4a).
2) Discard small objects in the image as noise using the Erode and Dilate morphological operations with kernel size 5×5 (Figure 4b).
3) Filter out objects smaller than 3000 pixels. The average pixel size of the emitter as captured by the ELD cameras is roughly 4500 when ELD detection starts, and larger afterwards.
4) Determine the bounding box of each remaining object, and filter out objects with height–width ratio smaller than 0.7 and larger than 1.3. The emitter is a cylinder of similar height and diameter, and its bounding box is roughly square from all viewpoints.
5) Select the object which has the highest red hue value, and perform hole filling (Figure 4c).

The position and orientation extraction step is based on the geometrical observation that when the cylinder is viewed from an angle, say 45°, the circular sides appear in the silhouette as approximately elliptic curves connected by straight lines. With this in mind, we extract the edges of the detected object (Figure 4d) using the Canny edge detector and apply the Hough transform to find straight lines in the edge image. We choose the line with the highest confidence as representing the emitter angle (ϕ_e) (Figure 4 center

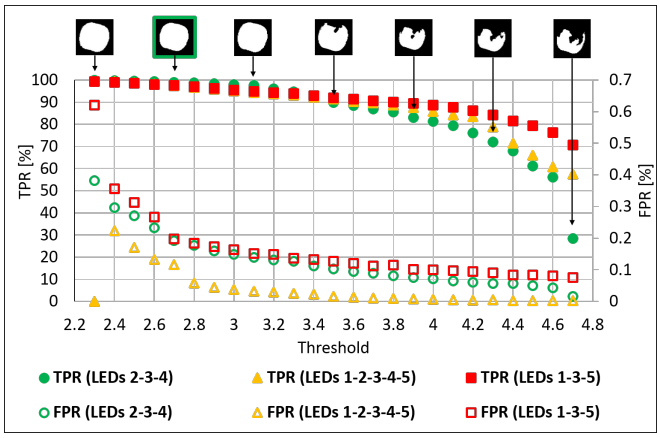

(a)

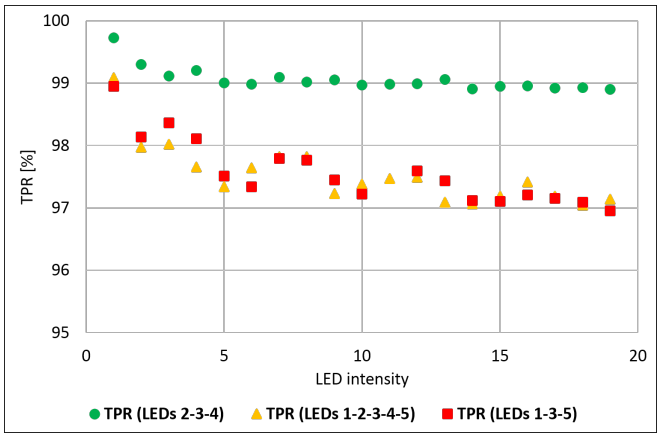

(b)

Fig. 5: True Positive Rate (TPR) and False Positive Rate (FPR) emitter detection sensitivity analysis. (a) Sensitivity to the threshold c on the sum of red–green and red–blue channel-ratio masks, and to the LED configurat on (1-2-3-4-5, 2-3-4, or 1-3-5), under LED intensity 5, as well as thumbnails of the detected masks (LED configuration 2-3-4). (b) Low sensitivity to LED intensity.

image).

We conducted sensitivity analysis of the threshold value c of the detection step over the range $[2.3, 4.7]$; of the lighting intensity over the range $[1, 19]$; and of different LED configurations: 1-2-3-4-5, 2-3-4, and 1-3-5 (Figure 1a). The lighting intensity value represent the PWM value where 255 is the full power of the LED (0.5w). For each light combination (intensity and configuration), a raw image was captured from each of the two ELD cameras in a grasp-ready position, processed using different threshold values, and evaluated against a manually segmented ground truth. We evaluated each setting on the resulting true-positive rate (TPR; ratio of correctly detected pixels to true emitter pixels) and false-positive rate (FPR; ratio of incorrectly detected pixels to non-emitter pixels).

The sensitivity analysis reveals how increasing the threshold c affects emitter detection. Figure 5a also shows thumbnails of the detected emitter under different threshold values. Based on these results we choose for the experiments of Section VI the threshold $c = 2.7$ for which the TPR is 99% and the FPR is relatively low (0.19%).

The LED intensity setting does not appear to affect emitter detection (Figure 5b), likely due to automatic light correction by the ELD cameras. The LED configuration was shown to have some impact on emitter detection (Figures 5a, 5b). We choose to use the middle LEDs (2-3-4), with intensity 2.

C. Mobile platform positioning algorithm

Before it can begin visual servoing, the robot must position its base in an initial position in front of the correct emitter where it can see the emitter with its in-hand camera. On the HSR, we use the in-base Hokuyo UST-20LX laser scanner for this initial positioning of the mobile platform. The laser scanner provides an estimated distance to the nearest floor-level obstacle in multiple directions from the platform, from which we infer the robot's base position and orientation (x_b, y_b, ψ_b) relative to the plant rack. The mobile platform positioning algorithm operates as follows:

1) Preprocess input data. The HSR laser scanner occasionally fails to provide input in the correct format, a vector of distance estimates in 963 directions. Invalid input is discarded.
2) Convert each input component (ψ_i, d_i) indicating an obstacle at distance d_i in direction ψ_i, to the (x_i, y_i) position of the obstacle, where $x_i = d_i \sin(\psi_i)$ and $y_i = d_i \cos(\psi_i)$.
3) Discretize the positions (x_i, y_i) (in centimeters) to positions in a centered 250×250 image, i.e., $(\lfloor x_i \rfloor + 125, \lfloor y_i \rfloor + 125)$.
4) Apply the Hough transform to detect lines in the image. The dominant straight line is assumed to be the plant rack's base surface.
5) For each line j detected:
   a) Isolate the line by applying its mask to the scan image.
   b) Compute the line length l_j, middle point (x_j, y_j), and angle ψ_j.
   c) Filter out lines of length differing from the known width of the rack (85cm in our experiments), i.e., having $l_j < 80$cm or $l_j > 90$cm.
   d) Select the remaining line with the highest confidence.

This procedure determines the plant rack's base surface to have its middle point and orientation at (x_j, y_j, ψ_j) in the robot's coordinate frame. This output can then be used to control the HSR to the desired position and orientation in the plant rack's coordinate frame, which is facing the rack perpendicularly at a fixed distance (43cm) in front of the specified emitter.

V. System Overview

A. Calibration process

ELD calibration establishes a correspondence between the detected position and orientation of the emitter in pixel

space (x_p, y_p, α_p) (Section IV-B) and the relative translation and pitch rotation between the gripper and the emitter, $(x_e - x_g)$, $(z_e - z_g)$, and $(\theta_e - \theta_g)$. Since grasping and rotating the emitter is only possible when the position and pitch of the emitter and the gripper are approximately in line, calibration determines the mapping from pixel-space position and orientation to gripper control needed for visual servoing.

Calibration is required each time that the ELD is attached to the robot's arm, and follows these steps:

1) Manually control the robot into a grasping position as shown in Figure 1c. In our experiments we control the HSR by teleoperation. The human operator should verify that the emitter grasp is sturdy and that the gripper's rotation axis is in line with that of the emitter.
2) Open the gripper without moving the arm, as shown in Figure 1b.
3) Detect the position and orientation of the emitter (x_p, y_p, α_p) in both ELD images, as described in Section IV-B.
4) Store the detected position and orientation as the pixel-space goal state of the emitter.

B. Emitter adjustment procedure

The robotic task in this work is to respond to a command $(x_e^i, y_e^i, z_e^i, \Delta\phi)$ by autonomously rotating the cap of the ith adjustable emitter by an angle of $\Delta\phi$. To do so, the robot must precisely position its gripper in the correct spatial position and orientation, which in turn requires the robot to position its base and arm accordingly. Unfortunately, the omnidirectional base of the HSR has large rotational errors in its motion.

To rely as little as possible on the HSR base, we fix its position early and perform the remaining motion using only the robotic arm. The procedure follows these steps:

1) Laser-based positioning step: using the algorithm presented in Section IV-C, the HSR base moves to a preset position relative to the known rough position of the emitter, in which the emitter should be visible to the in-hand camera. We apply PID control to the desired translation and rotation determined by the mobile platform positioning algorithm, until the HSR reaches the preset position of 43cm from the rack, facing perpendicular to the rack in front of the specified emitter.
2) Vision-based positioning step: the goal of this step is to position the HSR base more accurately, so that the rest of the reaching motion towards the emitter can be performed by the arm without moving the base. The robot makes a slight forward motion towards the plant rack, to a distance of 38cm from which the arm can reach the emitter. The difference from the previous step is that the lateral and vertical components of the motion are now determined by detecting the emitter in the in-hand camera image using standard red color extraction. We then apply PID controller to the pixel position of the emitter to bring it to the center of the in-hand image, fine-tuning for $y_g \simeq y_e$ and $z_g \simeq z_e$ (Figure 2). Laser-based positioning is still used to maintain the heading $\psi_b \simeq 0$ and control the forward motion on the x axis.
3) ELD-based reaching step: in this step the HSR base remains fixed, and only the arm is reaching for the emitter. We apply the emitter detection algorithm described in Section IV-B to the images captured by the ELD cameras to detect the emitter's position and orientation in pixel space (x_p, y_p, α_p), and average them between the two cameras. We then apply a PID controller to the difference between these values and the goal state store during calibration. The output of the PID controller is the intended motion of the gripper in coordinates (x_g, z_g, θ_g) ($y_g \simeq y_b$ is fixed by the base), which translates into control of the HSR joints according to: $\theta_1 = \arccos(x_g/L)$, $\theta_2 = \theta_g + 180^\circ - \theta_1$, and $z_{\text{arm}} = z_g - L\sin\theta_1$, where L is the length of the HSR arm link.

Using the two camera design contributes to the robustness of the system and in future application can be used to accurately measure the distance to the target. Following these positioning and reaching steps, the robot proceeds to grasp the emitter by closing its gripper, rotate the emitter cap by rolling the gripper the specified degree, releasing the grasp, and moving the base 15cm backward.

VI. Experiments

We experiment with the Toyota HSR to evaluate the device and methods proposed in Section V. We used nine houseplants arranged on a rack on three shelves as illustrated in Figure 6a. In order to evaluate the robustness of the proposed approach, we use three plant varieties, Basil, Thyme, and Mint, which diversifies the background colors and the layouts of the plants (Figure 6b). An irrigation tube of diameter 16mm is attached to each shelf (Figure 6c). Three Penta Angel adjustable emitters are attached to each irrigation tube, approximately at the center of each pot (Figure 6c). These emitters are red cylinders with 10mm height and 12mm diameter.

We begin each experiment by manually positioning the HSR in the vicinity of the plant rack. The HSR is then issued the sequence of commands $(x_e^i, y_e^i, z_e^i, \Delta\theta^\circ)_{i=1,\ldots,9}$ to the emitter adjustment procedure of Section V, whereby the robot should reach each emitter in turn, adjust it, back away, and continue to the next emitter. In each experiment we time separately the vision-based positioning step, the ELD-based reaching step, and the grasping step. A human experimenter marks each grasping attempt as a success or a failure.

In preliminary experiment we perform sensitivity analysis on the proportional gain parameters of the PID controllers mentioned in Section V-B. The initial proportional gains K_p, determined by a short process of manual trial-and-error tuning, were $K_p^{x_b} = 20$, $K_p^{y_b} = 5$, $K_p^{\psi_b} = 1$, $K_p^{x_g} = 1$, $K_p^{z_g} = 5$, and $K_p^{\theta_g} = 1$. The integral and derivative gains K_i and K_d were all set to 1, except for $K_d^{z_g} = 2$, and $K_i^{\theta_g} = K_d^{\theta_g} = 0$. The sensitivity analysis applies a multiplier

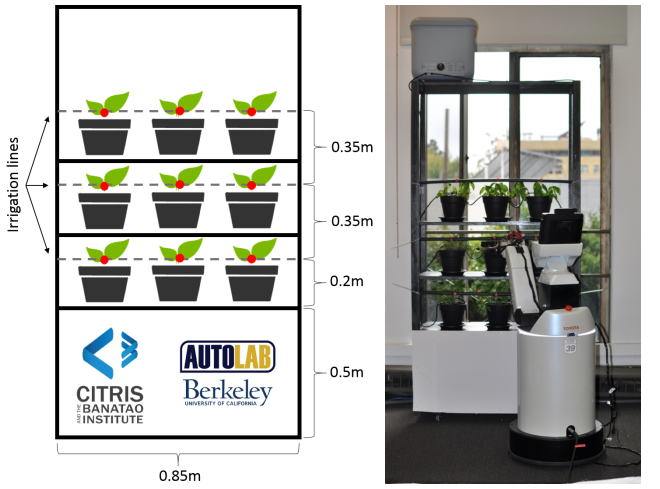

(a) (b)

(c)

Fig. 6: Plant rack setup. (a) Houseplants arrangement on the shelves. (b) Experimental setup of plant rack and Toyota HSR mobile robotic manipulator. (c) Three adjustable emitters attached to an irrigation tube.

in the range $[75\%, 120\%]$ uniformly to all proportional gains except $K_p^{\theta_g}$ (Figure 7).

Figure 7a reports the total time and success rate of the task, the latter dropping from close to 100% to about 60% as the gain is increased. Figures 7b and 7c break down the total time for the vision-based positioning and ELD-based reaching steps, respectively. The steps for grasping, rotation, release, and moving back add a total of about 3 seconds to each emitter's adjustment process. While the gain multiplier does not significantly affect the duration of the positioning step, it does slightly accelerate the reaching step. However, this minor improvement in task completion time comes at a high cost of frequent failures. Based on these results, we select 84% as the multiplier for the proportional controller gains, which are finally $K_p^{x_b} = 16.8$, $K_p^{y_b} = 4.2$, $K_p^{\psi_b} = 0.84$, $K_p^{x_g} = 0.84$, $K_p^{z_g} = 4.2$, and $K_p^{\theta_g} = 1$.

VII. Conclusions and Future Work

A novel approach to precision irrigation using the Toyota HSR robot in an indoor environment setup was developed. This paper explores how the Toyota HSR robot can support indoor precision irrigation using a novel low-cost Emitter Localization Device (ELD) mounted on the arm of the mobile manipulator to reach and adjust low-cost passive drip irrigation emitters. We describe the design of the device with stereo cameras and LED lighting and visual servoing

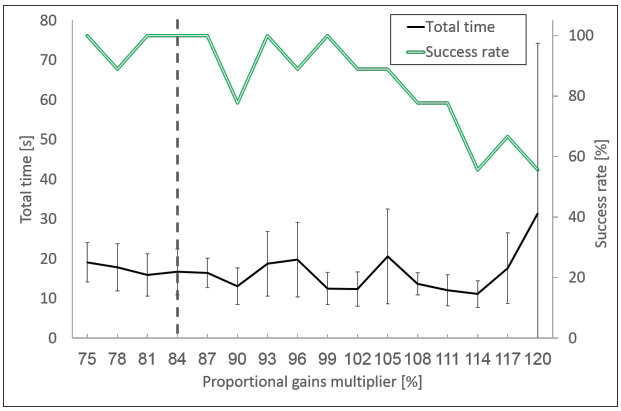

(a)

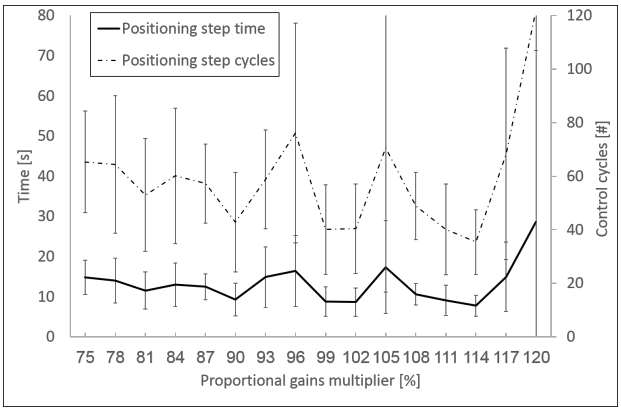

(b)

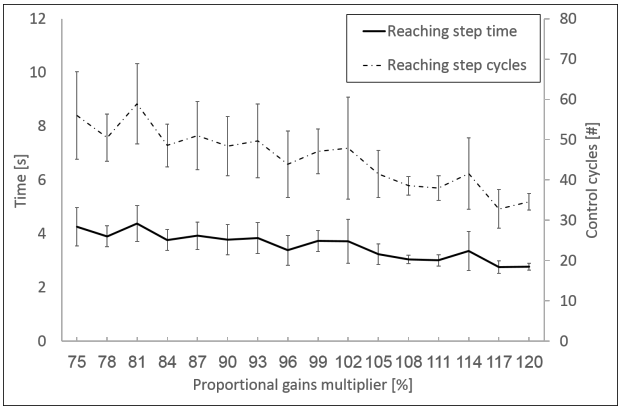

(c)

Fig. 7: Sensitivity of total time and success rate to the multiplier of proportional controller gains. The multiplier was applied uniformly to all proportional gains except $K_p^{\theta_g}$, and 84% was selected to maximize success rate. (a) Average total time (black) and success rate (green) for adjusting 9 emitters. (b) and (c) Total time and number of control cycles for the vision-based positioning and ELD-based reaching steps, respectively. We use 84 to obtain 95% success in 20sec.

algorithms and gain-tuning experiments that achieve 95% reliability in approx 20 seconds per emitter.

Future work will include more extensive experiments with

longer tasks and more plant and emitter types. By employing a differential approach to the two ELD cameras, we may improve robustness to base positioning and orientation. In future work we will also introduce a new ELD design with adjustable camera rotation, which would allow active tracking of the object and eliminate the need for a central camera such the HSR wide-angle in-hand camera. Another future direction is mounting an IR camera on the ELD to detect the water stress of each plant.

ACKNOWLEDGEMENTS

This research was performed at the AUTOLAB at UC Berkeley in affiliation with the Berkeley AI Research (BAIR) Lab and the CITRIS "People and Robots" (CPAR) Initiative. The authors were supported in part by Award 2017-67021-25925, RAPID: Robot-Assisted Precision Irrigation Delivery, from the USDA under the NSF National Robotics Initiative and by donations from Siemens, Google, Cisco, Autodesk, Amazon, Toyota Research, Samsung, and Knapp. Any opinions, findings, and conclusions or recommendations expressed in this material are those of the author(s) and do not necessarily reflect the views of the Sponsors. We thank our colleagues who provided helpful feedback and suggestions, in particular Adam Sequoia Beckman, Averell Wallach, and Menglong Guo. We also thank E. & J. Gallo Winery for their support of the work.

REFERENCES

[1] J.-P. Venot, M. Zwarteveen, M. Kuper, H. Boesveld, L. Bossenbroek, S. V. D. Kooij, J. Wanvoeke, M. Benouniche, M. Errahj, C. D. Fraiture, *et al.*, "Beyond the promises of technology: a review of the discourses and actors who make drip irrigation," *Irrigation and Drainage*, vol. 63, no. 2, pp. 186–194, 2014.

[2] F. Caniego, R. Espejo, M. Martın, and F. San José, "Multifractal scaling of soil spatial variability," *Ecological Modelling*, vol. 182, no. 3, pp. 291–303, 2005.

[3] D. Tseng, D. Wang, C. Chen, L. Miller, J. Viers, S. Vougioukas, S. Carpin, J. Aparicio Ojea, and K. Goldberg, "Learning to infer local soil moisture conditions from aerial agricultural images for automating precision irrigation," *Under review*, 2018.

[4] D. Despommier, "Farming up the city: the rise of urban vertical farms," *Trends in biotechnology*, vol. 31, no. 7, p. 388, 2013.

[5] K. Al-Kodmany, "The vertical farm: A review of developments and implications for the vertical city," *Buildings*, vol. 8, no. 2, 2018.

[6] N. Correll, N. Arechiga, A. Bolger, M. Bollini, B. Charrow, A. Clayton, F. Dominguez, K. Donahue, S. Dyar, L. Johnson, *et al.*, "Indoor robot gardening: design and implementation," *Intelligent Service Robotics*, vol. 3, no. 4, pp. 219–232, 2010.

[7] H. Nagaraja, R. Aswani, and M. Malik, "Plant watering autonomous mobile robot," *IAES International Journal of Robotics and Automation*, vol. 1, no. 3, p. 152, 2012.

[8] B. Al-Beeshi, B. Al-Mesbah, S. Al-Dosari, and M. El-Abd, "iplant: The greenhouse robot," in *Canadian Conference on Electrical and Computer Engineering (CCECE)*. IEEE, 2015, pp. 1489–1494.

[9] F. Taqi, F. Al-Langawi, H. Abdulraheem, and M. El-Abd, "A cherry-tomato harvesting robot," in *International Conference on Advanced Robotics (ICAR)*. IEEE, 2017, pp. 463–468.

[10] A. Agostini, G. Alenya, A. Fischbach, H. Scharr, F. Woergoetter, and C. Torras, "A cognitive architecture for automatic gardening," *Computers and Electronics in Agriculture*, vol. 138, pp. 69–79, 2017.

[11] D. V. Gealy, S. McKinley, M. Guo, L. Miller, S. Vougioukas, J. Viers, S. Carpin, and K. Goldberg, "Date: A handheld co-robotic device for automated tuning of emitters to enable precision irrigation," in *International Conference on Automation Science and Engineering (CASE)*. IEEE, 2016, pp. 922–927.

[12] R. Berenstein, O. B. Shahar, A. Shapiro, and Y. Edan, "Grape clusters and foliage detection algorithms for autonomous selective vineyard sprayer," *Intelligent Service Robotics*, vol. 3, no. 4, pp. 233–243, 2010.

[13] R. Aswani and N. Hema, "Robogardner: A low-cost system with automatic plant identification using markers," in *International Conference on Heterogeneous Networking for Quality, Reliability, Security and Robustness*. Springer, 2013, pp. 309–324.

[14] D. Hall, F. Dayoub, J. Kulk, and C. McCool, "Towards unsupervised weed scouting for agricultural robotics," in *International Conference on Robotics and Automation (ICRA)*. IEEE, May 2017, pp. 5223–5230.

[15] P. Lottes, M. Hörferlin, S. Sander, and C. Stachniss, "Effective vision-based classification for separating sugar beets and weeds for precision farming," *Journal of Field Robotics*, vol. 34, no. 6, pp. 1160–1178, 2017.

[16] O. Bawden, J. Kulk, R. Russell, C. McCool, A. English, F. Dayoub, C. Lehnert, and T. Perez, "Robot for weed species plant-specific management," *Journal of Field Robotics*, 2017.

[17] T. Botterill, S. Paulin, R. Green, S. Williams, J. Lin, V. Saxton, S. Mills, X. Chen, and S. Corbett-Davies, "A robot system for pruning grape vines," *Journal of Field Robotics*, vol. 34, no. 6, pp. 1100–1122, 2017.

[18] S. Bargoti and J. P. Underwood, "Image segmentation for fruit detection and yield estimation in apple orchards," *Journal of Field Robotics*, 2017.

[19] A. Silwal, J. R. Davidson, M. Karkee, C. Mo, Q. Zhang, and K. Lewis, "Design, integration, and field evaluation of a robotic apple harvester," *Journal of Field Robotics*, 2017.

[20] C. W. Bac, J. Hemming, B. Tuijl, R. Barth, E. Wais, and E. J. Henten, "Performance evaluation of a harvesting robot for sweet pepper," *Journal of Field Robotics*, 2017.

[21] F. A. Auat Cheein and R. Carelli, "Agricultural robotics: Unmanned robotic service units in agricultural tasks," *Industrial Electronics Magazine*, vol. 7, no. 3, pp. 48–58, 2013.

[22] B. Åstrand and A.-J. Baerveldt, "An agricultural mobile robot with vision-based perception for mechanical weed control," *Autonomous robots*, vol. 13, no. 1, pp. 21–35, 2002.

[23] T. Bak and H. Jakobsen, "Agricultural robotic platform with four wheel steering for weed detection," *Biosystems Engineering*, vol. 87, no. 2, pp. 125–136, 2004.

[24] L. Emmi, M. Gonzalez-de Soto, G. Pajares, and P. Gonzalez-de Santos, "New trends in robotics for agriculture: integration and assessment of a real fleet of robots," *The Scientific World Journal*, vol. 2014, 2014.

[25] R. Berenstein and Y. Edan, "Automatic adjustable spraying device for site-specific agricultural application," *IEEE Transactions on Automation Science and Engineering*, 2017.

[26] S. G. Vougioukas, "A distributed control framework for motion coordination of teams of autonomous agricultural vehicles," *Biosystems engineering*, vol. 113, no. 3, pp. 284–297, 2012.

[27] D. A. Johnson, D. J. Naffin, J. S. Puhalla, J. Sanchez, and C. K. Wellington, "Development and implementation of a team of robotic tractors for autonomous peat moss harvesting," *Journal of Field Robotics*, vol. 26, no. 6-7, pp. 549–571, 2009.

[28] S. N. Kumar, "Wireless agro robot for planting and irrigation control in farms," vol. 2, 2016.

[29] R. Berenstein and Y. Edan, "Human-robot collaborative site-specific sprayer," *Journal of Field Robotics*, vol. 34, no. 8, pp. 1519–1530, 2017.